doi:

V.P. KOSTYLYOV,[1] A.V. SACHENKO,[1] V.M. VLASIUK,[1] I.O. SOKOLOVSKYI,[1] S.D. KOBYLIANSKA,[2] P.V. TORCHYNIUK,[2] O.I. V'YUNOV,[2] A.G. BELOUS[2]

[1] V.E. Lashkaryov Institute of Semiconductor Physics, Nat. Acad. of Sci. of Ukraine *(41, Prosp. Nauky, Kyiv 03680, Ukraine; e-mail: vkost@isp.kiev.ua)*

[2] Vernadsky Institute of General and Inorganic Chemistry, National Academy of Sciences of Ukraine *(32/34, pr. Palladina, Kyiv 03142, Ukraine)*

SYNTHESIS AND INVESTIGATION OF THE PROPERTIES OF ORGANIC-INORGANIC PEROVSKITE FILMS WITH NON-CONTACT METHODS

PACS 73.50.Pz, 71.20.Rv, 88.40.H

Presented in this work are the results of our study of the photoelectric properties of perovskite $CH_3NH_3PbI_{2.98}Cl_{0.02}$ films deposited on a glass substrate using the spin-coating method. The unit cell parameters of the perovskite are determined using x-ray diffractometry. It is shown that the film morphology represents a net of non-oriented needle-like structures with significant roughness and porosity. In order to investigate the properties of the films obtained, non-contact methods were used, such as transmission and reflection measurements and the measurements of the spectral characteristics of the small-signal surface photovoltage. The non-contact method of spectral characteristics of the small-signal surface photovoltage and the transmission method reveal information about the external quantum yield in the films studied and about the diffusion length of minority carriers in the perovskite films. As a result of this analysis it has been established that the films obtained are naturally textured, and their bandgap is 1.59 eV. It is shown that in order to correctly determine absorption coefficient and the bandgap values, Urbach effect should be accounted for. Minority carriersќ diffusion length is longer than the film thickness, which is equal 400 nm. The films obtained are promising materials for solar cells and optoelectronic devices.

K e y w o r d s: surface photovoltage, perovskite film, diffusion length, transmission spectra, Urbach effect.

1. Introduction

An increase of the world energy consumption with hydrocarbons and atomic energy as primary sources has created a number of ecological, technological, social, and recently also economic problems. This has led to a growing of interest in the renewable energy sources. One of the most attractive and promising renewable sources of energy is photovoltaics, that is, direct transformation of solar radiation energy into electricity. Increasing the efficiency of photovoltaic energy conversion and decreasing the production cost per unit of energy remains an important problem since quite a long time. The promising candidates that can solve the above-pointed problems are solar cells (SCs) based on the organic/inorganic lead halide perovskite [1,2]. These are direct-bandgap materials, implying high optical absorption coefficient

value. SCs based on these materials belong to the second generation of thin-film SCs [3]. As compared to the traditional SCs based on monocrystalline silicon, their fabrication technology is simpler, because it does not require high temperatures, which reduces the price of these SCs. Besides, during the several years of their investigation, the efficiency of these cells has increased to 20.9% for the SC with the area of 1 cm^2 and to 23.7% for the area of 0.074 cm^2 [2, 4]. The most common methods to fabricate organic/inorganic lead halide perovskite are the so-called one-step solution deposition processes, in which all components are first solved in an organic solvent, such as N-dimethylformamide (DMF), then deposited on a substrate, and finally are thermally treated [5, 6]. Production of perovskite thin films is possible using many different deposition methods, such as spin-coating [7], deposition by dipping into a solution [8], blade-coating [9], sputtering [10], and vacuum deposition [11]. Also, the use of other solvents has been reported, such as butyrolactone [12] or dimethyl sulfoxide [13]. All the factors (deposition methods and solvents used) have a strong effect on the crystallization processes, therefore the films obtained are characterized by different morphologies (the shape and the size of the grains), and, correspondingly, by different crystal structure defects both on the grain boundaries and in the films. In polycrystalline films, grain size, their defect types and orientation strongly affect their optical and photoelectric properties. For photoconversion, optical and photoelectric characteristics are the most crucial. As a rule, they are studied in the already fabricated SCs, which consist of several layers in addition to the perovskite layer. As a result, the characteristics measured are integrated, that is, it is often difficult to single out the contributions of individual layers, which is important when production technologies are being developed. In [14] the roles of the selective contacts to methylammonium lead iodide chloride ($MAPbI_{3-x}Cl_x$) using surface photovoltage (SPV) spectroscopy have studied. By depositing and characterizing each layer at a time, have been shown that the electron-extracting interface is more than twice as effective as the hole-extracting interface in generating photovoltage, for several combinations of electrode materials. Their results illustrate the usefulness of SPV spectroscopy for study and characterization in perovskite-based photovoltaics. In that work surface photovoltage V_{SPV} was measured in a non-contact manner in a large signal mode (photovoltage values varied with-ing tens-hundreds mV), when surface photovoltage value V_{SPV} is much greater than the thermal voltage $V_{SPV} \gg kT/q$. Here k is Boltzmann's constant, T is the temperature, and q is the elementary charge. At $T = 300\ K$, $kT/q = 25.9\ mV$. For the first time, the method of spectral dependences of small-signal surface photovoltage ($V_{SPV} \ll kT/q$) to determine of the diffusion length of the minority charge carriers after Goodman in $CH_3NH_3PbI_3$ thin films and powders was used by Dietrich et al. [15]. Goodman's approach is valid for a semi-infinite plane-parallel sample with an optically mirror surface and is based on formula:

$$\Delta n = \frac{(1-R)I}{S + D/L} \frac{\alpha L}{1 + \alpha L}, \tag{1}$$

where Δn is the minority charge carriers concentration, R is the reflectance coefficient from the front surface, I is the photon flux per surface unity, $\alpha = \alpha(\lambda)$ is the absorption coefficient of the film, L is the minority charge carriers diffusion length. The expression (1) used to calculate the minority carrier diffusion length was obtained at the approximations $d \gg L$; $W \ll L$; $\alpha W \ll 1$; $\alpha(d - W) \gg 1$; $\Delta n \ll p_0$. Here d is the film thickness and W is the surface space-charge region width. Also since the experimentally measuring quantity is V_{SPV}, for obtaining proportionality $V_{SPV} \sim \Delta n$ it is necessary that the criterion of small signal $V_{SPV} \ll kT/q$ have to be done. In their study [15], the magnitude of the surface photovoltage signal did not exceed 120 μV, which indeed corresponds to the criterion $V_{SPV} \ll kT/q$. However, the second important criterion, $L \ll d$, was not met in their study. The authors obtained their results in the case of $L \approx d$, which leads to a significant error to determine L. Also and this is the main factor, the surface of the perovskite films is not specular, but has a certain relief thus the light rays direction in the film is not a perpendicular to surface. Therefore the Goodman approach has used by Dietrich [15] cannot, in principle, to give the exact diffusion length values of minority charge carriers in perovskite films with relief surface. Weng [16] also applied the Goodman's surface photovoltage spectroscopy method to determine the diffusion length of minority charge carriers in $CH_3NH_3PbBr_3$ crystals. In their measurements, all the criteria of the method were met, except the

small signal: the surface photovoltage values were $V_{SPV} = 70 - 200\ mV$, which is 3-4 times higher than kT/q, but not vice versa. Thus, there are no grounds for claiming accurate measurements of diffusion length. We can only talk about rough estimates of its value obtained in these works [16]. In present work, it is proposed to use the method of spectrally resolved small-signal surface photovoltage together with the measurements of the optical properties (transmission and reflection) for characterization and development of fabrication technologies of perovskite films with different microstructures. It will be shown that the spectral dependence of the small-signal surface photovoltage $V_{SPV}(\lambda)$ is proportional to external $EQE(\lambda)$ and internal quantum efficiency $IQE(\lambda)$ of photogeneration (imply photocurrent) [17, 18]. The methods proposed allow one to establish the mechanism of surface photovoltage formation, to obtain the bandgap value in a perovskite film as well as the diffusion length of the non-equilibrium minority charge carriers or photon path length values (if the absorption coefficient is known), and to estimate surface recombination velocity from the short-wavelength part of the photovoltage spectrum.

2. Experimental methods

Synthesis method Lead iodide PbI_2, methylammonium chloride CH_3NH_3Cl (C.P.), and methylammonium iodide CH_3NH_3I that was pre-synthesized were used as the input reagents [19]. In order to stabilize the perovskite structure, partial replacement of iodine with chlorine was carried out [20] using methylammonium chloride CH_3NH_3Cl (C.P.). Dried dimethylformamide (DMF, C.P.) was used as a solvent. To obtain the $CH_3NH_3PbI_{2.98}Cl_{0.02}$ films, the input reagents PbI_2, CH_3NH_3I, and CH_3NH_3Cl were dissolved in DMF in stoichiometric proportions and mixed for 1 hour at $70°C$. The synthesis was performed in a dry box. The so obtained transparent solution was then deposited onto a pre-cleaned substrate by spin-coating at 1200 rotations per minute during 30 seconds. Glass or ITO-coated glass (denoted hereafter as ITO/glass) were used as substrates. Thermal treatment of the films was carried out on a pre-heated stove at $90°C$ for 30 minutes. The products were characterized by x-ray powder diffraction taken on the apparatus DRON-4-07 (CuKα-radiation, $40\ V$, $18\ mA$) in the $2\Theta = 10-120°$ range with the step size of $0,02°$ and exposition time of $6s$. The unit cell parameters were determined using the Rietveld full-profile analysis method of the data.

Measurements of the physical characteristics. The spectral characteristics of the surface photovoltage were measured in the wavelength range $\Delta\lambda = 400-900\ nm$ on the perovskite $CH_3NH_3PbI_{2.98}Cl_{0.02}$ films deposited on glass with an ITO layer. The measurements were performed at a constant flux of photons of monochromatic light. The spectra obtained from these measurements are proportional to the external and internal quantum efficiency. Schematics of the experimental set-up for surface photovoltage measurements shows in Fig. 1. The light of a halogen lamp passed a monochromator, beam splitter and was directed onto the experimental sample. Surface photovoltage measurements were performed with a non-destructive method using a press-on ITO electrode with the area $\sim 7\times7\ mm^2$ deposited on mica of $\sim 5\ \mu m$ thickness. The spectral measurements were carried according to ASTM standards [21] on a set-up for the determination of spectral characteristics of photoconverters in the Center for testing of photoconverters and photoelectric batteries at the V.E. Lashkaryov Institute of Semiconductor Physics of the NAS of Ukraine. The transmission spectra in the wavelength range $\Delta\lambda = 400-900\ nm$ were measured on the perovskite $CH_3NH_3PbI_{2.98}Cl_{0.02}$ film samples deposited on glass without an ITO layer. As a photodetector, a silicon photodiode was used. The reflection coefficient was estimated for the wavelength of 632.8 nm. The measurements have revealed that reflection had diffusive character, and the reflection coefficient was quite small, estimated to be $\sim 5\%$.

3. Results and discution

To determine the unit cell parameters of the $CH_3NH_3PbI_{2.98}Cl_{0.02}$ material synthesized using the full-profile Rietveld method, the x-ray diffraction patterns of the single-phase samples were used, one of which is shown in Fig. 2. Calculations of the structure parameters indicate that this diffractogram corresponds to the tetragonal symmetry ($I4/mcm$ space group, № 140), which agrees with the literature data [22].

For the calculations, the atomic coordinates from this work were used for Pb (4c) 000; I1(8h) xy0; I2(4a) $00\frac{1}{4}$; C (16l) xyz; N (16l) xyz. For the

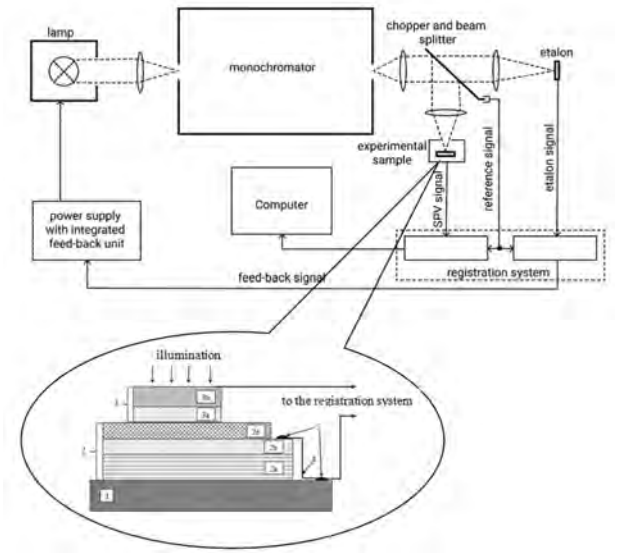

Fig. 1. Schematic of the experimental set-up for surface photovoltage (SPV) measurement.

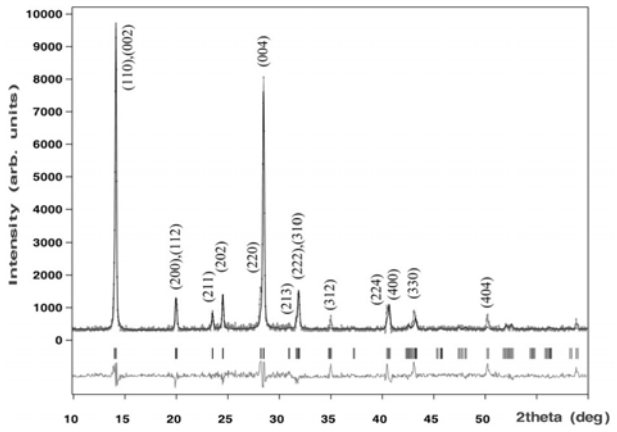

Fig. 2. Experimental (symbols) and theoretical (curves) x-ray diffractograms of a $CH_3NH_3PbI_{2.98}Cl_{0.02}$ film sample after thermal processing at 90°. The vertical lines indicate peak locations, with Miller indices given in the brackets. The difference curve is shown below.

$CH_3NH_3PbI_{2.98}Cl_{0.02}$ film the following lattice parameters were obtained: a = 0.8870(2) Å, c = 1.2669 (8) Å, V = 0.9968(7) Å^3. The microstructure analysis of the films obtained, see Fig. 3, shows that the ITO/glass substrate is incompletely covered by $CH_3NH_3PbI_{2.98}Cl_{0.02}$. The film morphology can be described as a net composed of non-oriented needle-like structures with a broad range of length to width ratio and significant film roughness and porosity.

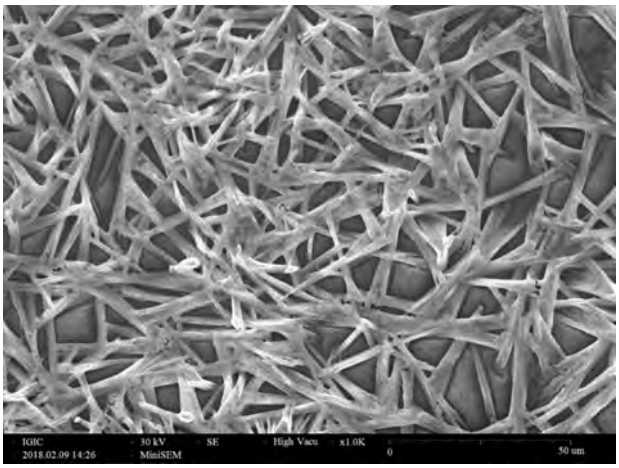

Fig. 3. $CH_3NH_3PbI_{2.98}Cl_{0.02}$ film microstructure after its thermal processing at 90°.

In general, the spectral dependence of the small-signal surface photovoltage $V_{SPV}(\lambda)$ can be described as [23]

$$V_{SPV}(\lambda) = A_1(\phi_s, \lambda)EQE(\lambda) = \\ = A_2(\phi_s, \lambda)IQE(\lambda), \quad (2)$$

where ϕ_s is the band bending on the illuminated side of the film, λ is the light wavelength, $A_1(\phi_s, \lambda)$, $A_2(\phi_s, \lambda)$ are the coefficients with the dimensions of Volts, $\alpha(\lambda)$ is light absorption coefficient, and $EQE(\lambda)$ and $IQE(\lambda)$ are the external and internal photocurrent generation quantum efficiencies. The relation between the external and internal quantum efficiencies for a non-absorbing film has the form [24]

$$EQE(\lambda) = (1 - R(\lambda))IQE(\lambda), \quad (3)$$

where $R(\lambda)$ is the reflaction coefficient. Thus

$$A_1(\phi_s, \lambda) = (1 - R(\lambda))A_2(\phi_s, \lambda). \quad (4)$$

According to [25], the dependence of the absorbance A_{nt} on λ near absorption edge for a parallel-plane specular structure with a single full reflection from backside has the form

$$A_{nt} = 1 - \exp(-2\alpha(\lambda)d), \quad (5)$$

and for the absorbance $A_t(\lambda)$ of a semiconductor substrate with nonspecular textured surfaces for the spectral region near the absorption edge ($\alpha d \ll 1$), the formula was obtained:

$$A_t(\lambda) = \frac{\alpha(\lambda)}{\alpha(\lambda) + \frac{1}{4dn_r^2}} = \left(1 + \frac{1}{4\alpha(\lambda)dn_r^2}\right)^{-1} \qquad (6)$$

It was also assumed that the reflection coefficient from the frontal surface is equal to 0, and from the back is equal to 1. Formula (6) describes the absorption edge to values $A_t(\lambda) = 0.9$ exactly. When $A_t(\lambda)$ is greater than 0.9, the error does not exceed 2% and rapidly decreases when $A(\lambda)$ approaches to 1 [26, 26]. Assuming that each absorbed photon generates one electron-hole pair and that there is no recombination (the minority carrier diffusion length L is much longer than the film thickness d), we can conclude that the formula for the internal quantum efficiency should have a similar form as (5, 6) namely:

$$IQE_{nt}(\lambda) = 1 - \exp(-2\alpha(\lambda)d) \qquad (7)$$

for a parallel-plane structure with specular surfaces and

$$IQE_t(\lambda) = \left(1 + \frac{1}{4\alpha(\lambda)dn_r^2}\right)^{-1} \qquad (8)$$

for a structure with nonspecular textured surfaces. Here d is the perovskite film thickness and n_r is its refraction index. Note that for a plane-parallel structure with specular surfaces when $L \leq d/3$ the internal quantum efficiency is well described by the well-known formula [28]

$$IQE(\lambda) = \frac{\alpha(\lambda)L}{1 + \alpha(\lambda)L} = \left(1 + \frac{1}{\alpha(\lambda)L}\right)^{-1}, \qquad (9)$$

where L is the minority carrier diffusion length and its value in this case can be found from the cutoff on the abscissa axis of the dependence of $IQE(\lambda)^{-1}$ on $\alpha(\lambda)^{-1}$ if $\alpha(\lambda)$ is known [21]. In the case of a textured or profiled surface, this same method will give significantly overestimated values of the diffusion length. As shown in [25, 29], the probability of photon absorption in long-wavelength region increases due to the Lambert scattering on a textured surfaces and increase of its path length from the value of $2d$ in a plane-parallel structure with a specular surface to the value of $4dn_r^2$ in a textured structure. This is the difference between the expressions (7) and (8). Texturing is known to be responsible for the higher values of the quantum efficiency and the short-circuit current, and hence of the photoconversion efficiency. An increase of the photoconversion efficiency is not only due to an increased photon path length, which leads to a broadening of quantum efficiency with λ and to its shifting towards the longer wavelengths; it is also due to a reduced frontal reflection coefficient value. This is related to the non-perpendicular light incidence on the textured elements of the structure, which leads to an increase in the photon path length due to multiple total internal reflection and to an increase in absorption in the long-wavelength region. It was established in [30, 31] that the absorption edge in the silicon HIT SCs and $FAPbI_3$-based SCs can be described by the generalized expression which differs from (8) by the presence of the parameter b:

$$IQE_t^*(\lambda) = \left(1 + \frac{b}{4\alpha(\lambda)dn_r^2}\right)^{-1}, \qquad (10)$$

where $b \geq 1$ is a non-dimensional parameter equal to the ratio of the longest photon path length possible, $4dn_r^2$ at ideal Lambertian light trapping to its real value. This ratio depends on the texturing quality (degree of light capture) and film thickness. We note that the case when the expression (8) with $b = 1$ is realized experimentally is rare. In particular, it was demonstrated in [30] that the experimental results for the textured silicon-based SCs and textured HIT SCs near the absorption edge can be described theoretically with a transformed expression of the form (10) with $b > 1$. Comparing (9) and (10), it is easy to see that the dependence of the inverse quantum efficiency on the inverse absorption coefficient is similar in both cases. The difference lies in the cut-off value on the a axis, which is equal to the diffusion length of minority carriers - L for a flat surface and to the average path length of photons $l_{ph} = 4dn_r^2/b$ for textured. Thus, in the case of a textured surface and diffusion lengths exceeding the thickness of the sample, we can determine the average path length of photons in the long-wavelength region of the spectrum near the absorption edge and the value of pa-

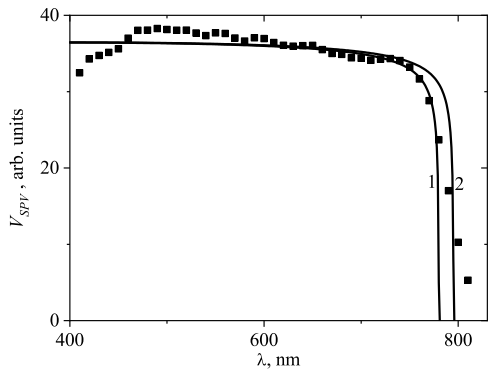

Fig. 4. Experimental (squares) and theoretical spectral dependencies (lines) of surface photovoltage $V_{SPV}(\lambda)$ calculated using expressions (2), (10) and (11) for bandgap values equal to 1.59 (curve 1) and 1.56 eV (curve 2).

rameter b. Because organic-inorganic perovskites are direct-bandgap semiconductors, the absorption coefficient $\alpha(\lambda)$ near the absorption edge is given by the formula [32]

$$\alpha(\lambda) = B\frac{\left(\frac{1239.7}{\lambda} - E_g\right)^{1/2}}{\frac{1239.7}{\lambda}}, \qquad (11)$$

where B is a constant, E_g is the bandgap value, and λ is the wavelength in nm. Fig. 4 shows the experimental dependence $V_{SPV}(\lambda)$ and the same dependencies calculated using expressions (2), (10) and (11) for bandgap values equal to 1.59 (curve 1) and 1.56 eV (curve 2). It is possible to see good agreement of the experimental curve with curve 1. From this figure, one can conclude that the bandgap in the film investigated is equal to 1.59 eV.

Experimental dependence of the absorption coefficient is very important for the analysis and interpretation of the experimental spectra of the small-signal surface photovoltage. We used in this work the most accurate dependence obtained in [33] over a wide range of wavelengths for the perovskite $CH_3NH_3PbI_3$. It is well known that the absorption edge in the structurally imperfect films is described by Urbach rule. The empirical absorption coefficient depends on the photon energy in this wavelength range as

$$\alpha_{ur} = \alpha_{ur0}\exp(E_{ph}/E_0), \qquad (12)$$

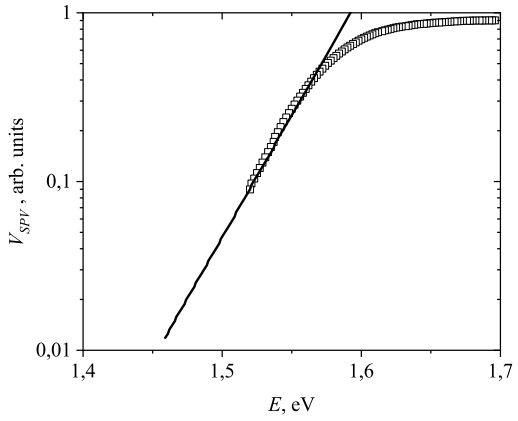

Fig. 5. Experimental spectral dependence of surface photovoltage $V_{SPV}(E)$ of the synthesized $CH_3NH_3PbI_{0.98}Cl_{0.02}$ films (squares). Line - theory (equation (12)). Urbach's energy is equal to 30 meV.

where α_{ur0} is the initial absorption coefficient, E_{ph} is photon energy, and E_0 is the characteristic energy, which is of the order of a few tens of meV for not too big deviations from the perfect films [34]. Figure 5 shows the experimental dependence of the small-signal surface photovoltage $log(V_{SPV})$ on the energy $E = 1239.7/\lambda$ (eV) normalized to value at $\lambda = 490$ nm and the theoretical dependence of the quantum yield calculated using formula (10). As can be seen from the figure, their agreement takes place in the region $\lambda > 790$ nm, if we put E_0 equal to 30 meV. The direction of the dependence of $V_{SPV}(E)$ in semilogarithmic coordinates for $\lambda > 790$ nm indicates the presence of the Urbach effect. Thus, in the analysis, we will use the $\alpha(\lambda)$ [32] dependence corrected for the Urbach effect (12) for $\lambda > 790$ nm.

Using the expressions (2) - (10) and corrected dependence $\alpha(\lambda)$ allows to build the low-signal surface photovoltage spectral curves and to determine the key parameters (namely, the perovskite film thickness d and the parameter b), at which they agree with the experiment near the absorption edge. More convenient for analysis are the spectral dependences of the small-signal surface photovoltage, constructed in coordinates V_{SPV}^{-1} versus $\alpha^{-1}(\lambda)$ [17, 18]. In these coordinates, the dependences (9) and (10) are straightened up in the long-wavelength region, and the cut-off on the abscissa axis $-\alpha_{cutoff}^{-1}(\lambda)$ is equal to the diffu-

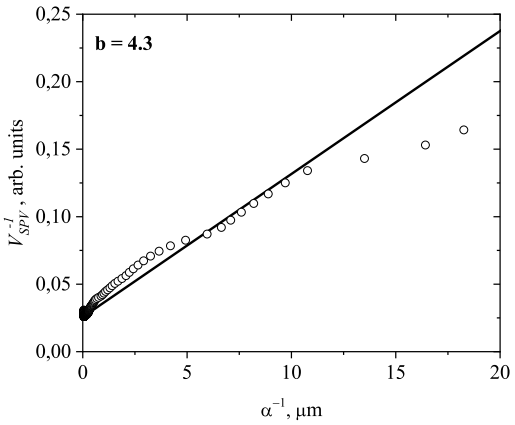

Fig. 6. Experimental (points) and calculated (line) dependencies $V_{SPV}^{-1}(\lambda)$ versus $\alpha^{-1}\lambda$, constructed using expression (10) and generalized values $\alpha(\lambda)$. Fitting parameters: $-\alpha_{cutoff}^{-1}(\lambda) = 2.1\ \mu m$, $d = 400\ nm$, and $b = 4.3$.

sion length L when $-\alpha_{cutoff}^{-1}(\lambda) \leq d/3$ according to (9) and $-\alpha_{cutoff}^{-1}(\lambda) = 4dn_r^2/b$ according to (10) otherwise. Fig. 6 shows the experimental and calculated dependencies of the inverse small-signal surface photovoltage V_{SPV}^{-1} on the inverse values of the absorption coefficient $\alpha^{-1}(\lambda)$, for the $CH_3NH_3PbI_{2.98}Cl_{0.02}$ film. Dependencies are constructed using the expression (10) and the generalized value of $\alpha(\lambda)$ [32]. As can be seen from Fig. 6, the experimental values at the absorption edge agree with the theoretical line well if we put $d = 400\ nm$, average path length $l_{ph} = 4650\ nm$ and $b = 4.3$. In this case, the cut-off on the abscissa axis $-\alpha_{cutoff}^{-1}(\lambda) = 2.1\ \mu m$, which significantly exceeds the thickness of the perovskite film $d = 0.4\ mkm$. If one uses the expression (7), the theory cannot fit the experiment for the film studied. Fig. 7 shows the same dependencies, but in coordinates surface photovoltage V_{SPV} versus wavelength λ. One can be seen a good agreement of theoretical (curve 1, expression (10)) and experimental (squares) dependencies. At the same time, when using expression (7) (plane-parallel structure, curve 2), there is no agreement between experiment and theory for the studied perovskite film in the absorption edge region.

Thus, it follows from this analysis that the film studied here captures light efficiently due to its natural profiling (texturing). This conclusion agrees with the microstructure data, see Fig. 3. The diffu-

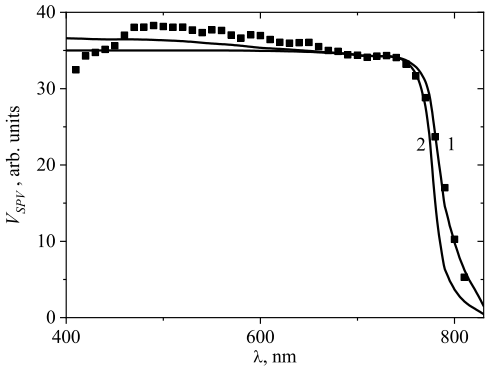

Fig. 7. Spectral dependencies $V_{SPV}(\lambda)$. Squares are experimental data, line (1) is a theoretical curve calculated using formulas (2) and (10), line (2) is a theoretical curve calculated using formulas (2) and (7). Parameters used: $d = 400\ nm$, $b = 4.3$.

sion length of the minority charge carriers L in the $CH_3NH_3PbI_{2.98}Cl_{0.02}$ films synthesized by us exceeds the thickness of sample d, because of spectra are described by expression (10). Let us note that the spectral curves of the small-signal surface photovoltage for film illumination from the opposite sides are close to each other. This provides an additional evidence of the high diffusion length (exceeding the film thickness), which, according to [35], are of the order of 1 μm in the samples with chlorine added. Let us now analyse the transmission spectra. Shown in Fig. 8 are the transmission spectra for a perovskite film on glass without ITO. The respective theoretical formulae are

$$T_{nt} = \frac{(1-R)^2 \exp(-\alpha d)}{1 - R^2 \exp(-2\alpha d)}, \tag{13}$$

and

$$T_t = (1-R)(1+\alpha(\lambda) l_{ph}(d,b))^{-1}. \tag{14}$$

The expression (13) should be applied for a plane-parallel structure, and (14) is valid for a textured structure (with the coefficient b taken into account).

Let us determine the transmission coefficient according to (14) for a film without the ITO layer using the generalized value for $\alpha(\lambda)$ for the perovskite $CH_3NH_3PbI_{2.98}Cl_{0.02}$ and the values $d = 400\ nm$ and $b = 4.3$ (curve 1). In this case, the agreement

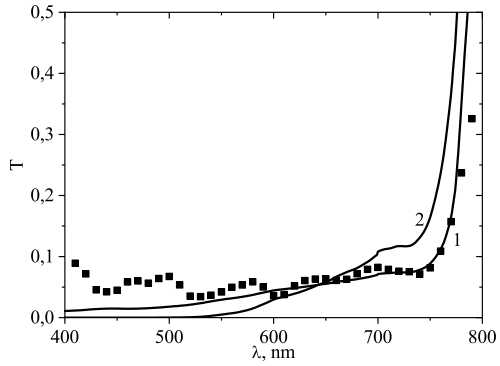

Fig. 8. Transmission spectra for film without ITO layer. Squares are experimental data. 1- Theoretical curve calculated using formula (14), 2 - theoretical curve calculated using formula (13). Parameters used: $d = 400\ nm$, $b = 4.3$.

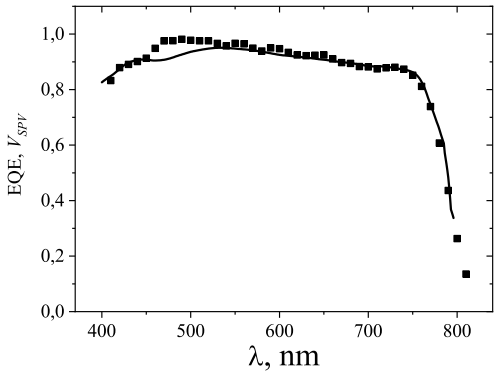

Fig. 9. Experimental (squares) and theoretical dependencies (line) small-signal photovoltage $V_{SPV}(\lambda)$ of the synthesized $CH_3NH_3PbI_{0.98}Cl_{0.02}$ films. Parameters used: $D_1 = 2.5\cdot10^{-2}\ m^2/s$, $L_1 = 2.4\cdot10^{-6}\ m$, $S_0 = 10^6\ m/s$, $d_1 = 100\ m$, $d = 400\ m$, $b = 4.3$.

between experiment and theory is quite good in the wavelength range from 500 nm to 800 nm. However, determination of the transmission coefficient according to (13) gives no agreement between the theoretical curve 2 and the experiment in the whole spectral range. Thus, the experimental transmission spectra of the film without the ITO layer also confirm that the film is naturally textured. Let us now consider the reasons of the $EQE(\lambda)$ decrease in the short-wavelength range in the perovskite SCs and the spectral dependence of the small-signal surface photovoltage $V_{SPV}(\lambda)$, see Fig. 9. As for the short-wavelength decrease of $V_{SPV}(\lambda)$, it is shown [32, 36] that this decrease has to do with the formation of a layer near the perovskite $CH_3NH_3PbI_{2.98}Cl_{0.02}$ surface with the carrier lifetime shorter than in the bulk. Shown in Fig. 9 are the experimental and theoretical dependences of $V_{SPV}(\lambda)$ normalized to the highest value for a perovskite films synthesized in this work.

Calculation of the curve $V_{SPV}(\lambda)$ for a $CH_3NH_3PbI_{2.98}Cl_{0.02}$ perovskite film, which gives a decrease at short wavelengths, was performed using the following formula for the effective surface recombination velocity

$$S_{eff}(\lambda) = \frac{D_1}{L_1}\times \\ \times \frac{S_0\frac{L_1}{D_1}cosh\left(\frac{1}{\alpha(\lambda)L_1}\right) + sinh\left(\frac{1}{\alpha(\lambda)L_1}\right)}{S_0\frac{L_1}{D_1}sinh\frac{1}{\alpha(\lambda)L_1} + cosh\left(\frac{1}{\alpha(\lambda)L_1}\right)} \quad (15)$$

taken from Ref. [36]. Here, D_1 and L_1 are, respectively, the diffusion coefficient and diffusion length in the surface layer of thickness d_1, and S_0 is the effective surface recombination velocity under the condition $\alpha d_1 \gg 1$. The theoretical $V_{SPV}(\lambda)$ curve was built using the following parameter values: $D_1 = 2.5\cdot10^{-2}$ cm^2/s, $L_1 = 2.4\cdot10^{-6}$ cm, $S_0 = 10^6$ cm/s, $d_1 = 100$ nm, $d = 400$ nm, $b = 4.3$. As seen from Fig. 9, the agreement between the experimental $V_{SPV}(\lambda)$ curve for the $CH_3NH_3PbI_{2.98}Cl_{0.02}$ film and the theoretical counterpart, it can be considered as satisfactory.

4. Conclusions

In the work, the efficiency of the method of spectrally resolved small-signal surface photovoltage was demonstrated together with the measurements of the optical properties (transmission and reflection) for the characterization of perovskite films. In particular, the methodology proposed allows one to consistently determine the bandgap value of a perovskite film, as well as its minority carriers diffusion length

in the case $L \leq d/3$ for a parallel-plane sample with specular surfaces or to estimate its value in the case of large diffusion lengths and /or textured surfaces. It has been shown that small signal surface photovoltage spectral dependences $V_{SPV}(\lambda)$ is proportional to external $EQE(\lambda)$ and internal quantum efficiency $IQE(\lambda)$ of photogeneration. It was shown that in the case of a textured surface and diffusion lengths exceeding the thickness of the sample, the cutoff on the abscissa axis of the dependence of the inverse surface photovoltage on the inverse absorption coefficient is equal to the average path length of the photons in the long-wavelength region of the spectrum near the absorption edge. A method is proposed for determining the average path length of photons and the value of parameter b. As a detailed analysis of the surface photovoltage spectra has shown, in the films mentioned above, Urbach effect plays an essential role near the absorption edge. One can obtain good agreement of the theory with experiment and to deduce an accurate value of the perovskite film bandgap of 1.59 eV only by taking this effect into account. It has been established by comparing of the experimental spectral curves of the small-signal surface photovoltage with the theory for textured structures that the films studied are naturally profiling. This agreement between the theory for textured structures and the experiment means that the diffusion length of the non-equilibrium charge carriers in the $CH_3NH_3PbI_{2.98}Cl_{0.02}$ perovskite films exceeds the film thickness. This is also supported by the results of a comparison between the spectra of the small-signal surface photovoltage obtained when the film was illuminated from the opposite sides. The value of the surface recombination velocity of the perovskite film was estimated, which turned out to be about 10^6 cm/s. It is established that the use of a transformed formula (10) allows one to make the theory consistent with the experiment not only near the absorption edge, but also to the EQE values up to $\sim$ 0.9.

1. M.A. Green, A. Ho-Baillie, and H.J. Snaith. The emergence of perovskite solar cells. *Nature Photonics* **8**, 7 (2014).
2. M.A. Green, Y. Hishikawa, E.D. Dunlop et al. Solar cell efficiency tables (Version 53). *Prog Photovolt Res Appl.* **27**, (2019).
3. M.A. Green. Third generation photovoltaics. Advanced solar energy conversion. *Springer* (2006).
4. W.S. Yang et al. High-performance photovoltaic perovskite layers fabricated through intramolecular exchange. *Science* **348**, 6240 (2015).
5. D. Song et al. Managing carrier lifetime and doping property of lead halide perovskite by postannealing processes for highly efficient perovskite solar cells. *The Journal of Physical Chemistry C* **119**, 40 (2015).
6. M.M. Lee, J. Teuscher, T. Miyasaka, T.N. Murakami, and H.J. Snaith. Efficient hybrid solar cells based on meso-superstructured organometal halide perovskites. *Science* **338**, 2 (2012).
7. B.-E. Cohen, S. Gamliel, and L. Etgar. Parameters influencing the deposition of methylammonium lead halide iodide in hole conductor free perovskite-based solar cells. *APL materials* **2**, 8 (2014).
8. J.-H. Im, I.-H. Jang, N. Pellet, M. Gratzel, and N.-G. Park. Growth of $CH_sNH_sPbl_s$ cuboids with controlled size for high-efficiency perovskite solar cells. *Nature nanotechnology* **9**, 11 (2014).
9. J. Burschka et al. Sequential deposition as a route to high-performance perovskite-sensitized solar cells. *Nature* **499**, 7458 (2013).
10. J.H. Kim, S.T. Williams, N. Cho, C.C. Chueh, and A.K.Y. Jen. Enhanced environmental stability of planar heterojunction perovskite solar cells based on blade-coating. *Advanced Energy Materials* **5**, 4 (2014).
11. K. Hwang et al. Toward large scale roll-to-roll production of fully printed perovskite solar cells. *Advanced Materials* **27**, 7 (2015).
12. J. Borchert, H. Boht, W. Franzel, R. Csuk, R. Scheer, and P. Pistor. Structural investigation of co-evaporated methyl ammonium lead halide perovskite films during growth and thermal decomposition using different PbX_2 (X = I, Cl) precursors. *Journal of Materials Chemistry A* **3**, 39 (2015).
13. J.-H. Im, C.-R. Lee, J.-W. Lee, S.-W. Park, and N.-G. Park. 6.5% efficient perovskite quantum-dot-sensitized solar cell. *Nanoscale* **3**, 10 (2011).
14. Lee Barnea-Nehoshtan, Saar Kirmayer, Eran Edri, Gary Hodes, and David Cahen. Surface Photovoltage Spectroscopy Study of Organo-Lead Perovskite Solar Cells. *J. Phys. Chem. Lett.* **5**, (2014).
15. Th. Dittrich, F. Lang, O. Shargaieva, J. Rappich, N.H. Nickel, E. Unger, B. Rech. Diffusion length of photo-generated charge carriers in layers and powders of $CH_3NH_3PbI_3$ perovskite. *Appl. Phys. Lett.* **109**, 073901 (2016).
16. J. Wang, E. Motaharifar, L.N.S. Murthy, et al. Revealing lattice and photocarrier dynamics of high-quality $MAPbBr_3$ single crystals by far infrared reflection and surface photovoltage spectroscopy. *J. Appl. Phys.* **125**, 025706 (2019);
17. L. Kronik, Y. Shapira. Surface photovoltage phenomena: theory, experiment, and applications. *Surface Science Reports* **37**, (1999).
18. D.K. Schroder. Surface voltage and surface photovoltage:

history, theory and applications. *Meas. Sci. Technol.* **12**, (2001).
19. J. Qiu et al. All-solid-state hybrid solar cells based on a new organometal halide perovskite sensitizer and one-dimensional TiO_2 nanowire arrays. *Nanoscale* **5**, 8 (2013).
20. A.G. Belous, O.I. V'yunov, S.D. Kobylyanskaya, A.A. Ishchenko, and A.V. Kulinich. Influence of Synthesis Conditions on the Morphology and Spectral-Luminescent Properties of Films of Organic- Inorganic Perovskite $CH_3NH_3PbI_{2.98}Cl_{0.02}$. *Russian Journal of General Chemistry* **88**, 1 (2018).
21. ASTM Standard F391-90a, "Standard Test Method for Minority-Carrier Diffusion Length in Silicon by Measurement of Steady-State Surface Photovoltage," *1996 Annual Book of ASTM Standards, Am. Soc. Test. Mat.*, West Conshohocken, PA, (1996).
22. Y. Kawamura, H. Mashiyama, and K. Hasebe. Structural study on cubic-tetragonal transition of $CH_3NH_3PbI_3$. *Journal of the Physical Society of Japan* **71**, 7 (2002).
23. A.V. Sachenko et al. Recombination characteristics of single-crystalline silicon wafers with a damaged near-surface layer. *Ukrainian journal of physics* **58**, 2 (2013).
24. C. Honsberg and S. Bowden. (30.10.2018). Quantum Efficiency (PVEducation ed.) [Internet]. Available: https://www.pveducation.org/pvcdrom/solar-cell-operation/quantum- efficiency.
25. T. Tiedje, E. Yablonovitch, G.D. Cody, and B.G. Brooks. Limiting efficiency of silicon solar cells. *IEEE Transactions on electron devices* **31**, 5 (1984).
26. M.A. Green. Lambertian Light Trapping in Textured Solar Cells and Light-Emitting Diodes: Analytical Solutions. *Prog. Photovolt: Res. Appl.* **10**, (2002);
27. S. Schafer and R. Brendel. Accurate Calculation of the Absorptance Enhances Efficiency Limit of Crystalline Silicon Solar Cells With Lambertian Light Trapping. *IEEE Journal of photovoltaics* **8**, 4 (2018).
28. A. Fahrenbruch and R. Bube. Fundamentals of solar cells: photovoltaic solar energy conversion. *New York: Elsevier*, (2012).
29. E. Yablonovitch. Statistical ray optics. *JOSA* **72**, 7 (1982).
30. A.V. Sachenko et al. Peculiarities of photoconversion efficiency modeling in perovskite solar cells. *Technical Physics Letters*, **43**, 7 (2017).
31. A.V. Sachenko et al. The Effect of Base Thickness on Photoconversion Efficiency in Textured Silicon-Based Solar Cells. *TechnicalPhysics Letters* **44**, 10 (2018).
32. K. Seeger. Semiconductor physics. Berlin, Germany: *Springer Science & Business Media* (2013).
33. Stefaan De Wolf, J. Holovsky, S.-J. Moon, P. Lo?per, B. Niesen, M. Ledinsky, F.-J. Haug, J.-H. Yum, and C. Ballif. Organometallic Halide Perovskites: Sharp Optical Absorption Edge and Its Relation to Photovoltaic Performance. *J. Phys. Chem. Lett.* **5**, (2014).
34. J.D. Joannopoulos and G. Lucovsky. The Physics of Hydrogenated Amorphous Silicon II: Electronic and Vibrational Properties. Berlin, Germany: *Springer Science & Business Media* (2008).
35. C. Wehrenfennig, G.E. Eperon, M.B. Johnston, H.J. Snaith, and L.M. Herz. High Charge Carrier Mobilities and Lifetimes in Organolead Trihalide Perovskites. *Advanced Materials* **26**,10 (2013).
36. V.P. Kostylyov, V.G. Lytovchenko, A.V. Sachenko, T.V. Slusar, V.V. Chernenko, Features of solar cells and solar silicon wafers surface photovoltage spectral dependences in the short-wave absorption region, *in Proceedings 28 European Photovoltaic Solar Energy Conf. and Exhib.*, Paris, France, 30 Sept.-04 Oct., 2013, pp. 1715-1718.

Received 23.03.20

В.П. Костильов, А.В. Саченко, В.М. Власюк, І.О. Соколовський, С.Д. Кобилянська, П.В. Торчинюк, О.І. В'юнов, А.Г. Білоус

СИНТЕЗ І ДОСЛІДЖЕННЯ ВЛАСТИВОСТЕЙ ПЛІВОК ОРГАНО-НЕОРГАНІЧНИХ ПЕРОВСКІТІВ БЕЗКОНТАКТНИМИ МЕТОДАМИ

В роботі наведено результати дослідження фотоелектричних характеристик плівок перовскіту $CH_3NH_3PbI_{2,98}Cl_{0,02}$, нанесених на скляну підкладку методом spin-coating. З використанням рентгенівських методів дослідження визначено параметри елементарної комірки перовскіту та показано, що морфологія плівок описується як сітка неорієнтованих голкоподібних структур із значною шорсткістю та пористістю. Для дослідження властивостей отриманих плівок використовувались безконтактні методи, зокрема, вимірювання пропускання і відбивання та метод спектральних залежностей малосигнальної поверхневої фотонапруги. Показано, що метод спектральних залежностей малосигнальної поверхневої фотонапруги та метод пропускання містять інформацію про зовнішній квантовий вихід в досліджуваних плівках та про довжину дифузії неосновних носіїв у плівках перовскіту. В результаті аналізу спектрів встановлено, що отримані плівки є природно профільованими, а їх ширина забороненої зони становить 1.59 . Показано, що при визначенні залежності коефіцієнта поглинання та ширини забороненої зони слід враховувати ефект Урбаха. Довжина дифузії неосновних носіїв заряду більша за товщину плівок, яка дорівнює 400 . Отримані плівки є перспективними для розробки на їх основі ефективних сонячних елементів.